

Received May 08, 2020; reviewed; accepted September 28, 2020

Preparation of amphoteric modified bentonite from calcium-based bentonite for adsorption of anionic dye: The importance of sodium-modification pretreatment

Hang Yin ¹, Zijie Ren ^{1,2}, Huimin Gao ^{1,2}, Weiyi Han ¹, Junfang Guan ¹

¹ School of Resources and Environmental Engineering, Wuhan University of Technology

² Hubei Key Laboratory of Mineral Resources Processing and Environment, Wuhan University of Technology

Corresponding author: renzijie@whut.edu.cn (Z. Ren)

Abstract: To understand the influence of sodium-modification pretreatment on the adsorption of anionic dye by amphoteric modified bentonite, three kinds of adsorbent materials, including sodium-modified bentonite, amphoteric modified calcium-based bentonite and amphoteric modified bentonite pretreated by sodium modification, were firstly synthesized and characterized, and afterwards their adsorption performance and mechanism for a form of anionic dye, Acid Yellow 11, were investigated comparatively. The crystalline phases, hydration property, surface charge characteristic and functional groups of prepared modified bentonite were characterized and evaluated by X-ray diffraction swelling volume, Zeta potential and Fourier transform infrared spectroscopy, respectively. The sodium modification expanded the interlayer space of montmorillonite, released the internal surface area and improved the hydration performance of bentonite. Due to the replacement of Na⁺ for Ca²⁺, the probability of interlayer cations overflowing from the interlayer space and exchanging with the amphoteric modifier increases. Therefore, the content of interlaminar organic material in amphoteric modified bentonite pretreated with sodium-modification pretreatment was higher than that in unpretreated amphoteric modified bentonite. The hydration and dispersibility were significantly stronger, and the adsorption capacity of acid dye was also better. The findings of this investigation suggest that sodium modification pretreatment is very positive and necessary in the process from sodium–amphoteric modification.

Keywords: calcium-based bentonite, sodium modification pretreatment, amphoteric modification, anionic dye

1. Introduction

The textile dyeing and finishing industry is a pillar industry in many countries and regions worldwide. China has been ranked as the world's largest textile and dyed fabric producer for several consecutive years. In 2019, the production of yarn in mainland China was 28.921 million tons, and that of cloth was 57.56 billion meters, which were 6.1% and 17.6% less than in 2018, respectively (National Bureau of Statistics of the PRC, 2020). Among them, from January to October 2019, the output of dyed cloth produced by enterprises above a designated size reached 44.169 billion meters, an increase of 4.51% over the same period in 2018 (Liang, 2020). The huge industrial scale also brought huge environmental pressures. Even if the latest national emission standards are strictly implemented (Ministry of Ecology and Environment of the PRC, 2012), the annual generation of dyeing wastewater exceeds 700 million tons (40% reuse). With the continuous strengthening of environmental protection awareness, the government has issued a series of guiding policies for the dyeing industry, with a view to achieving healthy industrial development while reducing pollutant emissions and environmental hazards (Ministry of Ecology and Environment of the PRC, 2017; Ministry of Ecology and Environment of PRC, 2018). However, as of September 2019, according to the list of enterprises conforming to the standards

and conditions of the printing and dyeing industry (2017 edition) published by the ministry of industry and information technology in two batches, there were only 22 enterprises conforming to the standards (Ministry of Industry and Information Technology of the PRC, 2019). Compliance emissions have become a bottleneck, restricting the development and even survival of the dyeing industry. Dyeing wastewater has deep chroma, poor biochemical properties and is difficult to treat. The currently studied methods for treating dyeing wastewater include biochemical oxidation, biodegradation and photocatalytic degradation (Hameed and Ismail, 2020; Lum et al., 2020; Oliveira et al., 2020), functional microbial flocculant flocculation (Wang et al., 2020), ozone and fungal combined treatment methods (Vanhulle et al., 2008). Among them, the physical and biochemical oxidation methods represented by sewage treatment plants are still the mainstream of industrial applications (Wang et al., 2011; Yuan et al., 2020), and there are also studies that try to improve the treatment efficiency and the stability of the treatment (Vives et al., 2003). Compared with other treatment methods, the decolorization effect of the adsorption is stable, and the resistance to wastewater quality changes is better (Zhuang et al., 2009). The adsorbent is cheap and has a wide range of sources (Malik, 2004; Ebrahimi et al., 2013; Georgin et al., 2016), so the adsorption method has a stronger competitiveness in industrial production applications.

Due to the existence of exchangeable hydrated cations (Na^+ , Ca^{2+} , etc.) in the interlayer domain of montmorillonite particles, the bentonite naturally has a good adsorption performance for cationic dyes (basic dyes) (Leodopoulos et al., 2015) and, furthermore, it also endows bentonite with good modifiable ability (Rawajfih and Nsour, 2006; Haghseresht et al., 2009; Hou et al., 2011; Arellano-Cardenas et al., 2013). Bentonite can be divided into many types according to the type of interlayer hydrated cations, including calcium-based bentonite and sodium-based bentonite, as well as hydrogen-based, aluminum-based, sodium-based, calcium-based and other types of bentonite. Bentonite is widely distributed in many countries worldwide (Aronson and Lee, 1986; Benito et al., 1998; Mitchell et al., 2004; Kirali and Lacin, 2006; Afolabi et al., 2017; Belousov and Krupskaya, 2019). Among them, China's bentonite resources are very rich. As of 2017, the identified reserves of bentonite ore resources in mainland China have been 3.06 billion tons (National Bureau of Statistics of PRC, 2019), of which 70% is calcium-based bentonite (Wu et al., 2016). Compared with natural sodium-based bentonite, calcium-based bentonite has poor adsorption properties and modifiable properties, but calcium-based bentonite has large reserves and cheap prices. It is more cost-effective as an adsorbent and has more potential for use in industrial applications.

Amphoteric surfactants contain both anionic and cationic hydrophilic groups in the same molecule, so they can both donate protons and accept protons (Yan et al., 2004). Amphoteric modified bentonite is obtained by amphoteric surfactants intercalated into the montmorillonite layer through ion exchange or adsorbed on the outer surface of montmorillonite particles due to hydrophobic bonding (LI, 2012). The amphoteric surfactant has a hydrophobic long carbon chain at one end and anionic and cationic hydrophilic groups at the other end, so that the amphoteric modified bentonite has better adsorption performance for nonionic organic pollutants and cationic pollutants (Meng et al., 2007; Pang et al., 2008; Sun and Zhu, 2010). However, there are some limitations in the study of amphoteric modified bentonite: First, most studies on amphoteric modified bentonite have selected high-quality sodium-based bentonite as the object of modification in order to obtain better adsorption performance. However, few studies on amphoteric modified bentonite choose calcium-based bentonite as the object of modification, and the effects of sodium modification pretreatment on the adsorption performance of amphoteric modified bentonite have been neglected. Second, the adsorption studies of amphoteric modified bentonite are mainly focused on nonionic organic pollutants and cationic pollutants, but few anion organic pollutants.

Therefore, in this study, high-grade natural calcium-based bentonite was used as the modification object, and medium-long chain amphoteric surface-active BS-12 was used as the modifier to prepare an amphoteric modified bentonite. The acid dye AY11 was used as the adsorption object to evaluate the adsorption performance of modified bentonite on anionic organic matter, with a view to achieving the following research objectives: (1) preparation and characterization of amphoteric modified bentonite based on calcium-based bentonite; (2) explore the adsorption mechanism of amphoteric modified bentonite on anionic organic matter; (3) investigate the mechanism of the influence of sodium

modification pretreatment on the modifiable properties of bentonite and the adsorption properties of amphoteric modified bentonite.

2. Experimental

2.1. Materials and Reagents

Bentonite minerals were supplied from a bentonite mine in Huludao, Liaoning, China. Raw bentonite (RB) was purified by free settling with a classification size of 10 μm and dried. After drying, the sample was crushed in an agate mortar to produce bentonite concentrate (BC).

Dodecyl dimethyl betaine (BS-12, CAS: 683-10-3), an amphoteric surfactant produced by the Qingdao Uoslf Chemical Technology Co., Ltd., was used as the amphoteric modifier. Fig. 1a shows the chemical structure of BS-12. The C.I. Acid Yellow 11 (AY11, CAS:6359-82-6), a form of acid azo dye, was purchased from Hubei Baidu chemical Co., Ltd., China. Fig. 1b shows the chemical structure of AY11.

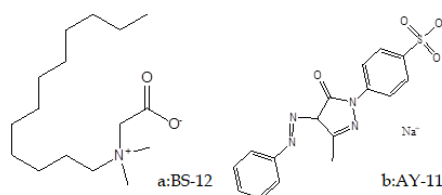


Fig. 1. Chemical structure of AY11 and BS-12

2.2. Adsorbent preparation

To prepare the Na-modified bentonite (NB), 100 g of BC powder was transferred to a quartz conical flask blended with a 500 ml solution of Na_2CO_3 with 1 wt%, and stirred for 30 min at 60°C. The conical flask was sealed with a polyethylene film and aged at 50°C for 72 h, dried at 95°C and then ground into powder form and screened by a sieve size of 45 μm . Then, 10 g of the NB and BC were transferred to two quartz conical flasks blended with 200 ml distilled water and stirred at 60°C. Then, 2 ml dodecyl dimethyl betaine (BS-12) solution (35wt%) was dropped into the slurry at a rate of 1 ml/min, stirring for 4 h at a constant temperature of 60 °C. The conical flask was sealed and aged at 50°C for 72 h. Finally, the bentonite slurry was washed 10 times with distilled water and then dried at 80 °C and ground into powder form and screened by a sieve size of 45 μm . The two prepared adsorbents were Amphoteric Modified Na-Bentonites (AMNB) and Amphoteric Modified Ca-Bentonites (AMCB). The preparation flow is shown in Fig. 2.

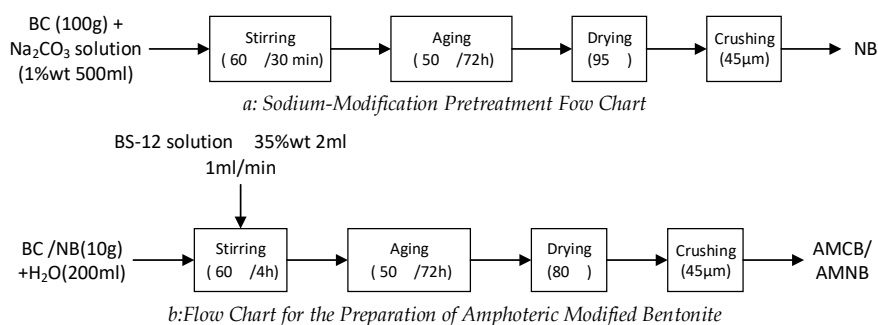


Fig. 2. Adsorbent preparation flow chart

2.3. Adsorption experiments

For adsorption experiments, the desired concentration and dosage of AY11 and adsorbent were transferred into a 100 ml quartz conical flask and shaken for a certain time in temperature controlled by a water bath shaker (SHA-BA, XINBAO, Jintan, China). The solid phase was separated from the solution using a high-speed centrifuge (H2050R-1, CENCE Instruments Co., Ltd., Hunan, China). Then, the absorbance of the residual AY11 in the supernatant was measured at 398 nm, using a UV-Vis spectrophotometer (A-360, AOE Instruments Co., Ltd., Shanghai, China). The concentration of the

residual AY11 was determined using the linear regression equation ($y = 0.0158x + 0.008$, $R^2 = 0.9999$), obtained by plotting a calibration curve for AY11 over a concentrations range. The percentage removal of pigment was calculated using the following equation:

$$\text{Removal efficiency(\%)} = \frac{(C_0 - C_t)}{C_0} \times 100 \quad (1)$$

where C_0 and C_t are the initial and at time t concentrations (mg/L) of AY11, respectively. The amount of adsorbed AY11 at equilibrium q_e (mg/g) was calculated using the formula:

$$q_e = \frac{(C_0 - C_e)V}{m} \quad (2)$$

where C_e is the equilibrium concentration of AY11 solutions (mg/L), V is the volume of pigment solution (L) and m is the mass of adsorbent (g).

2.4. Testing methods

2.4.1. Zeta potential measurement

For zeta potential measurement, the samples were ground in an agate mortar. The particle size of the ground powder was below 2 μm , as measured by the Leica DMLP Microscope. In total, 30 mg of ground minerals was mixed with 50 mL DI water in a beaker. After stirring for 2 min, HCl or NaOH was added to adjust the slurry pH and stirred for another 6 min. The slurry was then injected into a Tiselius cell in a Zeta Plus Zeta Potential measurement unit. Each sample was measured three times and the average zeta potential was reported.

2.4.2. Infrared spectroscopic analysis

Fourier transform infrared spectroscopy (FTIR) analysis was conducted by a Nicolet iS10 FTIR Spectrometer. A small amount of mineral sample was mixed with KBr and ground in an agate mortar. The ground powder was pressed into a pellet and then transferred into the spectrometer for measurement.

2.4.3. XRD

X-ray diffraction patterns were obtained with X-ray diffractometer D/Max-III A (RIGAKU, Japan) with monochromatic Cu K α radiation, at an angle range of 3°–70° and a rate of 0.02 °/s.

2.4.4. Cation exchange capacity (CEC)

The method of CEC measurement was based on GB/T 20973-2007 (General administration of quality supervision, inspection and quarantine of the PRC and Standardization administration of the PRC, 2007). The method is as follows:

A total of 1.00 g of the dried bentonite sample was weighed, put it into a 50 mL centrifuge tube and then covered and weighed (m_1). Then, 30 mL barium chloride solution (0.1 mol/L) was added, shook mechanically for 1 h, centrifuged at 3000 g relative centrifugal force for 10 min, poured out in suspension in a 100 mL volumetric flask. The above process was repeated more than twice and add 100 mL volume of suspension. The bottle was adjusted to 100 mL with barium chloride solution. This was named filtrate A. The bentonite was dispersed and precipitated with 30 mL barium chloride solution (0.0025 mol/L), shook mechanically for 1 h and left to stand for more than 5 h. Then, the bentonite was centrifuged at 3000 g relative centrifugal force for 10 min, and the supernatant was poured out. The centrifugal test tube of precipitated bentonite was weighed and covered (m_2), then 30 mL of magnesium sulfate solution (0.0200 mol/L) was added to disperse the precipitated bentonite, shook mechanically for 1 h and left to stand for more than 5 h. Then, it was centrifuged for 10 min under the condition of a relative centrifugal force of 3000 g and poured onto the upper layer. The clear liquid was filtered through a 7 cm diameter filter paper into an Erlenmeyer flask. This was named filtrate B. The above steps were followed without adding bentonite to test as a blank control sample. Then 0.200 mL of filtrate B and control blank test solution were transferred from the Erlenmeyer flask to a 100 mL volumetric flask, 10 mL lanthanum nitrate solution (10 mg/L) was added and diluted to the mark with water. At the wavelength of 285.2 nm, the absorbance was measured on an atomic absorption spectrophotometer with an air acetylene

flame, and the magnesium concentration of filtrate B (C_1) and the magnesium concentration of the blank test solution (C_{b1}) were calculated from the standard curve. The cation exchange capacity (CEC) was calculated according to the formula:

$$CEC = \frac{(C_{b1} - C_2)3000}{m} \quad (3)$$

$$C_2 = C_1(30 + m_2 - m_1)/30 \quad (4)$$

where CEC is the cation exchange capacity of the sample (mmol/100g), C_{b1} is magnesium concentration of blank test solution (mmol/L), C_2 is magnesium concentration in filtrate B after correction (mmol/L), m is the mass of the sample (g), C_1 is magnesium concentration in filtrate B (mmol/L), m_1 is mass of centrifugal tube and dry sample (g), m_2 is mass of centrifugal tube and wet sample (g).

2.4.5. Swell volume (SV)

The method of SV measurement is based on SNT 0990-2001 (General administration of quality supervision, inspection and quarantine of the PRC, 2001). The method is as follows:

First 2.0 g of the sample was weighed and added to a measuring cylinder with a stopper of about 60 ml of water added in several times. The sample was shook during adding to avoid the agglomeration of the sample. After all the samples were added, 25 mL of hydrochloric acid (1mol/L) was added, shook for about 1 min and diluted to 100 mL with water. This was left to stand for 24 h and the scale value at the interface of the precipitate was read. The swell volume was expressed as the expansion volume/sample weight (mL/g) and was calculated according to the formula:

$$A = \frac{B}{m} \quad (5)$$

where A is the SV of the sample (mL/g), B is expanded volume of bentonite (mL), m is the mass of the sample (g).

2.4.6. Methylene Blue Index (MBI)

The method of MBI measurement is based on GB/T 20973-2007. The method is as follows:

First $0.2 \text{ g} \pm 0.001 \text{ g}$ of bentonite sample that had been dried at $105^\circ\text{C} \pm 3^\circ\text{C}$ for 2 h was weighed and placed in a 250 ml conical flask pre-filled with 50 ml water. This was made wet, and dispersed on a magnetic stirrer for 5 minutes. Then, 20ml of 1% sodium pyrophosphate solution was added and stirred for 2 to 3 minutes. Then, the sample was heated on an electric furnace to slight boiling for 2 min, before removal and cooling to $25 \pm 5^\circ\text{C}$.

Methylene blue standard solution was added dropwise with a burette while stirring. For the first time, about two thirds of the total amount of methylene blue solution was added, stirring for 2 minutes to fully react, and then 1 to 2 ml was added each time. After stirring for 30 seconds, a drop of test solution was taken with a glass rod and quantified at a medium speed. On the filter paper, we observed whether or not there was a light blue halo around the blue spots. We continued to drip the methylene blue solution. When the blue halo started to appear, we continued stirring for 2 minutes, and then dipped a drop of test solution on the medium-speed quantitative filter paper with a glass rod and observed whether the light blue halo remained. In the event that the light blue halo did not appear, we continued. Methylene blue solution was carefully added dropwise. When a light blue halo appeared after stirring for 2 minutes, this indicated that the end point had been reached, and the titration volume was recorded. The methylene blue index is calculated according to the formula:

$$MBI = \frac{395.81VC}{1000m} \times 100 \quad (6)$$

where MBI is methylene blue index (g/100g), C is concentration of methylene blue solution (mol/L), V is the titer of methylene blue solution (mL) and m is the mass of the sample (g).

3. Results and discussion

3.1. Characterization of modified bentonite

Fig. 3 shows the main phase compositions of the PB and BC analyzed by X-ray diffraction patterns analysis (XRD). Raw bentonite (RB) is made up of montmorillonite, feldspar and calcite. The d spacing,

a typical characteristic peak of the 001 plane (d001) of montmorillonite, was 15.43Å, indicating that this bentonite sample belongs to calcium bentonite. After purification, the calcite in the sample is almost completely removed, but a small amount of feldspar remains.

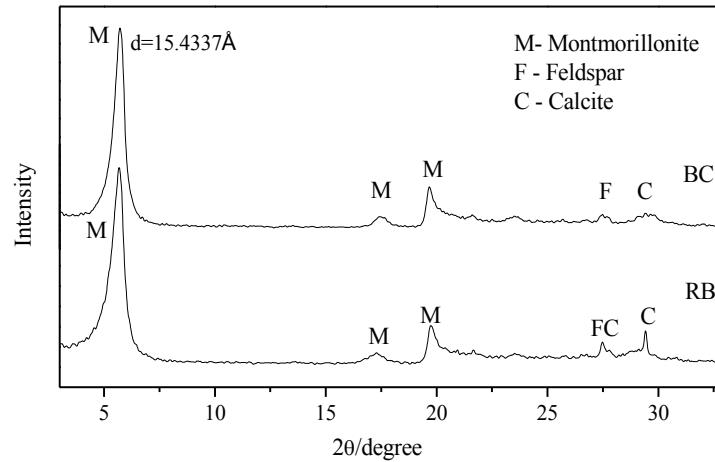


Fig. 3. XRD diffraction patterns of the Raw bentonite and BC

Table 1 lists the chemical composition of the RB and BC. The content of Al_2O_3 and MgO in BC increased, and the other components decreased. The decrease in CaO could be related to the removal of calcite, while SiO_2 , K_2O and Na_2O were related to feldspar.

Table 1. Chemical composition of RB and BC

Component	SiO_2	Al_2O_3	MgO	CaO	Fe_2O_3
RB (wt. %)	61.887	17.616	4.970	2.365	1.580
BC (wt. %)	61.542	18.971	5.352	2.183	1.215
Component	K_2O	Na_2O	TiO_2	P_2O_5	L.O.I.*
RB (wt. %)	0.599	0.254	0.137	0.135	10.458
BC (wt. %)	0.553	0.205	0.113	0.034	9.832

The MBI showed that the montmorillonite content in the purified sample BC increased from 82% to 90%.

Fig. 4 shows the XRD patterns of the four samples. As seen in Fig. 3, the Na-modified treatment of BC leads a decrease in d001 values and changes in basal reflections from $d_{001} = 15.43 \text{ \AA}$ to $d_{001} = 12.44 \text{ \AA}$, resulting from the replacement of interlayer Ca^{2+} by Na^+ , which indicates that the calcium bentonite modified to be sodium bentonite. The CEC of BC was 92.05 mmol/100g, and that of NB was 97.87 mmol/100g. The increase in CEC indicated that the total amount of cation exchange increased due to the replacement of calcium ions by sodium ions, which could also prove the success of sodium modification. The influence of amphoteric organic modifier BS-12 on bentonite was also reflected by the change in d001 value. The d001 values increased from $d_{001} = 15.43 \text{ \AA}$ of BC to $d_{001} = 16.41 \text{ \AA}$ of AMCB, and from $d_{001} = 12.44 \text{ \AA}$ of NB to $d_{001} = 14.74 \text{ \AA}$ of AMNB, caused by the intercalation of amphoteric surfactant. By comparing the change in the d001 value before and after the amphoteric modification, it can be found that the d001 value of both calcium bentonite and Na-modified bentonite increases after the amphoteric modification of BS-12. This indicates that both calcium bentonite and Na-modified bentonite can be modified by the intercalation of an amphoteric organic modifier, such as BS-12. In addition, the d001 value of NB that had been Na-modified as a pretreatment increased more after amphoteric modification than that of BC. The difference in d001 values between AMCB and AMNB is caused for two reasons. On the one hand, after BS-12 enters the BC and NB layers, it cannot completely replace the original interlayer hydrated cations, and the remaining hydrated cations continue to affect the interlayer spacing. On the other hand, due to the large difference in hydration properties between NB and BC, the amount of BS-12 entering the layers is different. Generally speaking, the greater the amount of modifier entering the interlayer, the greater the increase in d001 value (Xiao et al., 2020a).

The hydration performance of NB is better than that of BC, so more BS-12 enters the interlayer of NB, making the value of NB d001 increase larger than that of BC.

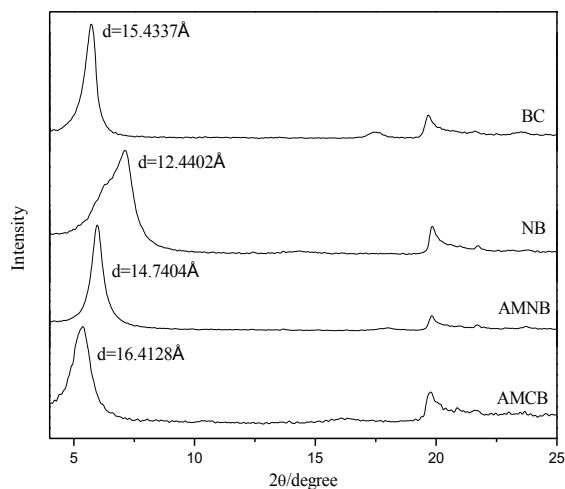


Fig. 4. XRD patterns of the four samples

3.2. Batch adsorption tests

AY11 is a widely used acidic anionic dye with moderate molecular weight, easily soluble in water, stable in acid and alkali resistance, strong color rendering, and stable coloration. It is representative of an azo dye. The adsorption test with AY11 can reasonably and accurately evaluate the adsorption capacity of modified bentonite for acidic anionic dyes.

In order to estimate the equilibrium contact time for adsorption of AY11 onto BC, NB, AMCB and AMNB, the adsorption study was carried out at different time interval ranges from 0 to 120 min under certain conditions and the results are shown in Fig. 5a. It can be seen from Fig. 5a that BC can hardly adsorb AY11. The adsorption performance of modified bentonite on AY11 is AMNB > NB > AMCB. AY11 was rapidly adsorbed by AMCB and AMNB with an increasing contact time of up to 15 min, which then became constant as the contact time went by. The adsorption rate was faster at the beginning because the AY11 molecules were adsorbed by the exterior surface at an early stage, and then after their saturation, were adsorbed by the interior surface of the adsorbent (Amin, 2009). However, the adsorption of AY11 on NB quickly reached saturation (≤ 15 min), and then the adsorption curve is nearly flat and unchanged without an obvious phase change, indicating that the adsorption of NB on AY11 is different from the adsorption mechanism of AMCB/AMNB on AY11. For further study, 60 min was selected as the equilibrium time.

The effects of initial concentration of AY11 on the amount of adsorbed pigment (Fig. 5b) were discussed in detail. Within the range of the initial concentration of AY11, the adsorption capacity of AMNB is always significantly better than that of AMCB and NB, which once again confirms the superiority of the adsorption performance of composite modified bentonite. When the initial concentration of AY11 was low (10–50 mg/L), there was no significant difference between the adsorption capacity of AMCB and NB for AY11. When the initial concentration was higher (60–80 mg/L), NB shows better adsorption performance. During the initial concentration increase in AY11, it was not adsorbed by unmodified bentonite. However, the adsorption capacity of the other three modified bentonites increased with the increase in the initial concentration in the range 10–80 mg/L at the same temperature. These amounts can be higher with higher concentration of AY11 for the same amount of adsorbent. This results from an increase in mass transfer driving force due to the concentration gradient developed between the bulk solution and surface of the adsorbent (Purkait et al., 2006).

3.3. Adsorption kinetics, isotherms and thermodynamics

In order to investigate the adsorption process of AY11 onto NB, AMCB and AMNB kinetics data were checked through the pseudo-first-order and pseudo-second-order model (Ho and Mckay, 1999). The

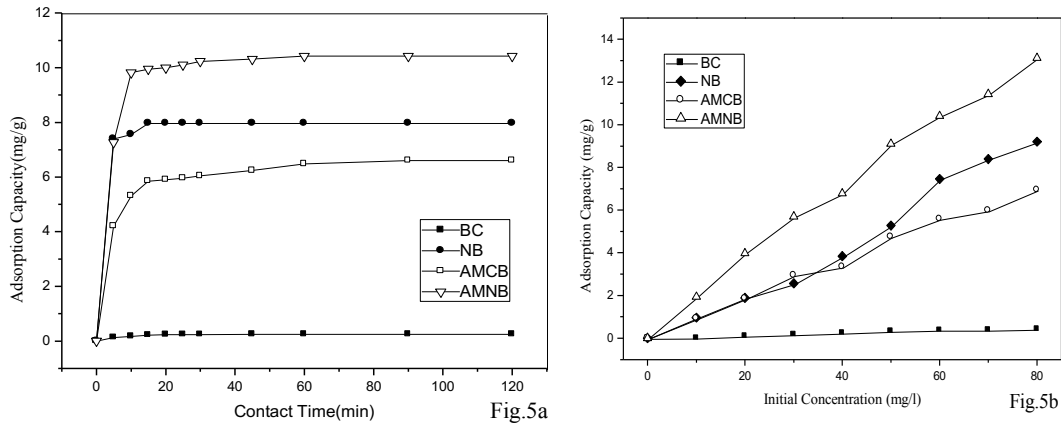


Fig. 5. Effect of contact time on AY11 adsorption capacity (a) (dose of adsorbent = 1 g/L, AY11 = 50 mg/L, temperature = 298 K, pH = 6.5) and effect of initial concentration on AY11 adsorption capacity (b) (dose of adsorbent = 1 g/L, contact time = 60 min, temperature = 298 K, pH = 6.5)

comparison of pseudo-first-order and pseudo-second-order is shown in Table 2. Among them, the relative error was calculated by dividing the absolute value of the difference between the two sets of values by the set of values with a high correlation coefficient. It can be seen from Table 2 that, for the quasi-first-order kinetics model, the correlation coefficients of the three samples' nonlinear fittings are significantly higher than those of the linear fitting, indicating that the nonlinear fitting results of the quasi-first-order kinetics of the samples are better than the linear fitting results. The linear fitting correlation coefficient of quasi-second-order kinetics is slightly better than that of nonlinear fitting, but the difference is small. The regression coefficient value (R^2) of linear fitting is all higher than 0.999, and the relative error of Q_e and K is smaller than that of quasi-first-order kinetics fitting, indicating that the three samples followed the pseudo-second-order kinetics model better.

Table 2. Kinetic parameters for the adsorption of AY11 (308 K)

308 K	Parameter	Nonlinear fitting	Linear fitting	Relative error
pseudo-first-order				
	Equation	$q_t = q_e(1 - e^{-k_1 t})$	$\ln(q_e - q_t) = \ln q_e - k_1 t$	
NB	q_e (mg/g)	7.92	14.34	81.06%
	k_1 (min^{-2})	0.5247	0.6152	17.25%
	R^2	0.9978	0.8786	
AMCB	q_e (mg/g)	6.21	2.93	52.82%
	k_1 (min^{-2})	0.2084	0.0530	74.57%
	R^2	0.9882	0.8699	
AMNB	q_e (mg/g)	10.24	3.89	62.11%
	k_1 (min^{-2})	0.2566	0.0916	64.30%
	R^2	0.9957	0.8282	
pseudo-second-order				
	Equation	$q_t = \frac{k_2 q_e^2 t}{1 + k_2 q_e t}$	$\frac{t}{q_t} = \frac{1}{k_2 q_e^2} + \frac{t}{q}$	
NB	q_e (mg/g)	8.06	6.29	28.14%
	k_2 (g/mg min)	0.0271	0.0255	6.27%
	R^2	0.9989	0.9999	
AMCB	q_e (mg/g)	6.72	5.15	30.49%
	k_2 (g/mg min)	0.0527	0.0377	39.79%
	R^2	0.9977	0.9998	
AMNB	q_e (mg/g)	10.84	9.33	16.18%
	k_2 (g/mg min)	0.0177	0.0115	53.91%
	R^2	0.9896	0.9998	

The experimental results of isothermal adsorption, shown in Fig. 6a–c, are adsorption isotherms of NB, AMCB and AMNB at 298, 308 and 318 K, respectively, and the initial concentration range is 10–80 mg/L.

Adsorption isotherms are characterized by certain constant parameters associated with surface characteristics, the affinity of the adsorbent and the adsorption capacity of the adsorbent, which can be used to evaluate the feasibility of this process for a given application and determine the adsorbent dosage required (Purkait et al., 2006; Zheng et al., 2017).

In this study, to describe the adsorption equilibrium, Langmuir and Freundlich isotherm models were used to fit the experimental results for the AY11 adsorption onto NB, AMCB and AMNB. All isotherms can be linearized, and then the parameters can be determined graphically or by linear regression (Periasamy and Namasivayam, 1995; Otker and Akme Mehmet-Balcoglu, 2005).

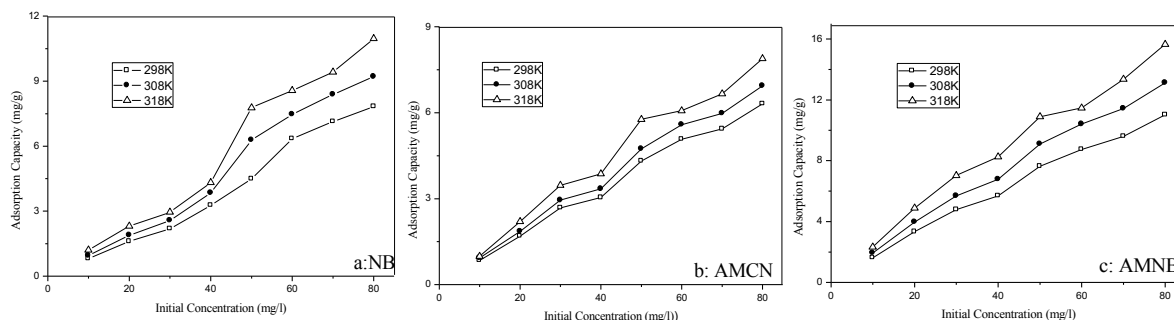


Fig. 6. Effect of initial concentration of AY11 and temperature on the amount (dose of adsorbent = 1g/L, contact time = 60 min)

The Langmuir isotherm is applicable to homogeneous sorption, where the sorption of each sorbate molecule onto the surface has equal sorption activation energy. The isotherm properties by fitting Langmuir and Freundlich equations are shown in Table 3. As can be seen, the RL values obtained when fitting the Langmuir equation were less than 1, indicating the great affinity of the NB, AMCB and AMNB for AY11. The magnitude of the exponent n gives an indication of the favorability of adsorption when fitting the Freundlich equation. Generally, n in the range 2–10 represents good, 1–2 represents moderately difficult, and less than 1 represents poor adsorption characteristics. The Freundlich equation describes heterogeneous systems and reversible adsorption. This is not restricted to the formation of monolayers. The isotherms model results of three samples showed similar rules: the correlation coefficients (R^2) of the linear form of the Langmuir model were higher than those of the Freundlich model, which means that the adsorption process of AY11 onto NB, AMCB, and AMNB follow the Langmuir model better. The thermodynamic model results of three samples showed similar behavior: the adsorption process has a spontaneous nature as indicated by the negative values of ΔG° . Physical adsorption may have played an important role in AY11 uptake for the ΔG° values in the range of -20 to 0 kJ mol^{-1} (Li et al., 2011). The positive value of ΔH° reveals endothermic adsorption, and this is in agreement with the expected higher negative values of ΔG° at higher temperatures. The positive value of ΔS° suggests increased randomness at the solid–solution interface during the adsorption (Acemioglu, 2004).

The thermodynamic parameters provide in-depth information on the energetic changes associated with the adsorption process, and the adsorption thermodynamic parameters of the three samples are shown in Table 4.

Table 3. Isotherm properties of AY11 adsorption when fitting Langmuir and Freundlich equations

308 K	Langmuir				Freundlich		
	$Q_{m,ca}$ (mg/g)	K_L (L/mg)	R^2	R_L	K_F (mg/g) / (mg/L) $^{1/n}$	n	R^2
NB	29.50	3.832×10^{-3}	0.9882	0.77–0.96	0.072	0.84	0.9700
AMCB	25.84	4.468×10^{-3}	0.9970	0.74–0.96	0.128	1.04	0.9915
AMNB	50.25	6.642×10^{-3}	0.9961	0.65–0.94	0.436	1.16	0.9915

Table 4. Thermodynamic parameters for the adsorption

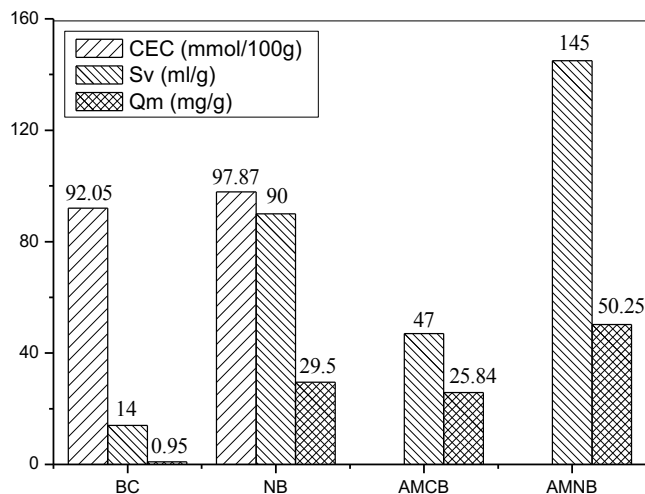
Sample	ΔG (kJ mol ⁻¹)			ΔS (J K ⁻¹ mol ⁻¹)	ΔH (kJ mol ⁻¹)
	286 K	298 K	308 K		
NB	-3.97	-4.43	-4.73	16.02	6.18
AMCB	-4.83	-5.32	-5.58	18.77	6.31
AMNB	-2.61	-3.10	-3.86	13.52	11.17

3.4. Adsorption mechanisms

The test results of CEC, SV and Q_m are shown in Fig. 7. Comparing the SV of BC and NB, it can be seen that the swelling performance of bentonite was significantly improved by sodium modification, and the swelling performance of NB was 640% that of BC. This means that the degree of dispersion of NB particles in water is much higher than that of BC. Meanwhile, after the Na-modified bentonite particles are dispersed in water, the water-soil system formed has high stability. In addition, BS-12 modification can also improve the swelling properties of bentonite. The swelling capacity of AMNB increased by more than 50% compared with NB, and that of AMCB increased by 165% compared with BC. This indicates that amphoteric modification can greatly improve the dispersion property of bentonite and improve the stability of the water-soil system. However, by comparing the SV of AMNB and AMCB, it can be seen that the effects of sodium modification on the dispersion properties of bentonite was greater than that of ambidextrous amphoteric modification. At the same time, Fig. 7 shows the positive correlation between bentonite's adsorption capacity for AY11 and swelling performance—the higher the swell volume (SV), the stronger the adsorption capacity (Q_m). For bentonite, the higher the swelling performance and the better the dispersibility, the more favorable it is for the occurrence of adsorption, which is consistent with the test results. It follows that the effects of sodium modification on the swelling performance of bentonite is particularly significant. Therefore, in order to improve the adsorption of bentonite, the pretreatment of sodium modification is necessary.

To better understand the effect of modification on bentonite, the electro-kinetic phenomenon of mineral suspensions was investigated. Fig. 8 shows the zeta potential of four samples as a function of pH.

In the pH range of 2–8, the surface of four samples always accumulated negative charges. With the increase in pH, the negative charge on the surface of the particles showed an increasing trend, and the change trend of the surface charge of the four samples was consistent. By comparing the surface zeta potential changes in BC and NB, it can be found that sodium modification greatly increases the amount of surface negative charge of bentonite. The larger the surface potential, the stronger the electrostatic repulsion between the colloidal particles, the less the possibility of mutual aggregation and precipitation, and the better the stability of the system. The zeta potential changes and the swelling capacity of NB and BC are consistent with this rule (Barast et al., 2017). After the modification of BS-12,

Fig. 7. CEC, SV, Q_m of the four samples

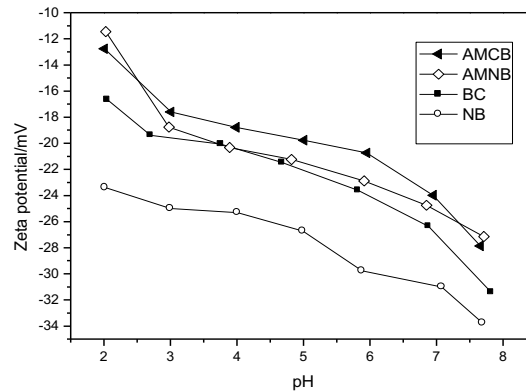


Fig. 8. Zeta potentials of the four samples

the negative surface charges of BC and NB were reduced, indicating that BS-12 had similar effects on BC and NB. On the other hand, although the surface electronegative properties of AMNB and AMCB are weaker than those of NB and BC, their swelling performance is stronger, indicating that the stability of organic modified bentonite in the water–soil system no longer depends only on the ions' charge. After the intercalation of organic modifiers, the colloidal swelling in bentonite's swelling mechanism is amplified. Therefore, although the negative charges on the surface of AMCB and BC decreased compared to AMNB and NB, their swell volume increased (Yang, 2018).

The FT-IR spectra of the four samples are shown in Fig. 9. It can be seen from Fig. 9 that the FT-IR spectra of the four samples have many similarities—of which, in the high-frequency region, the absorption band at about 3617 cm^{-1} belongs to the stretching vibration mode of OH- in montmorillonite Al-Al-OH and Al-Mg-OH ($\nu_{\text{OH-A}}$) (Bianchi et al., 2013). The interlaminar water stretching vibration of montmorillonite is around 3418 cm^{-1} , while the bending vibration is around 1637 cm^{-1} , and the absorption band is strong (Dawodu and Akpomie, 2014). The infrared absorption band at 1035 cm^{-1} is attributed to the Si-O stretching vibration modes in Si-O-Si, Si-O-Al, and SiO₂ in montmorillonite ($\nu_{\text{Si-O-B}}$) (Madejova, 2003). The infrared absorption band at 916 cm^{-1} is attributed to the bending vibration mode of OH- in montmorillonite Al-Al-OH ($\delta_{\text{OH-1-A}}$) (Slany et al., 2019). The infrared absorption band at 845 cm^{-1} is attributed to the bending vibration mode of OH- in montmorillonite Al-Mg-OH ($\delta_{\text{H-2-A}}$). The infrared absorption band at 789 cm^{-1} is attributed to Si-O-Si symmetric stretching mode corresponding to SiO₂ in montmorillonite ($\nu_{\text{O-Si-O-A}}$) (Santos et al., 2020a). The band at 520 cm^{-1} represents the coupling vibration of Si-O-M (M means cation) at the octahedron of montmorillonite (Zhu et al., 2016) and the absorption band at 466 cm^{-1} represents the bending vibration of Si-O-Si ($\delta_{\text{Si-O-Si}}$) (Saidi et al., 2012). These absorption bands are generated by Si-O vibration, OH and interlayer water vibration, and Mg-O/Al-O vibration in bentonite, and they are observed in the infrared spectrum of bentonite (Madejova, 2003).

The differences in the FT-IR spectra of the four samples are as follows: Compared with BC, the wide absorption band of NB at 1454 cm^{-1} belongs to the CO₃²⁻ stretching vibration mode, which is caused by the Na₂CO₃ in the sodium modification (Yang et al., 2020). The spectra of NB and BC are very similar, especially in the low-frequency region of the lattice bending vibration band, the peak shape and intensity are almost identical, indicating that Na⁺ only replaces the Ca²⁺ between the layers of montmorillonite in BC, but has no effect on Mg²⁺ and Al³⁺ in the montmorillonite lattice. In the AMCB and AMNB spectra, -CH-symmetric (ν_{sCH}) and anti-symmetric (ν_{asCH}) stretching vibration bands appear at 2926 cm^{-1} and 2854 cm^{-1} in the intermediate frequency region (Ren et al., 2018), indicating that BS-12 was inserted between montmorillonite layers. The AMNB spectrum has a small absorption peak at 722 cm^{-1} , which is attributed to the out-of-plane bending vibration peak (ω_{CH}) of the carbon chain -CH₂- (Santos et al., 2020b).

Three small and dense finger-type absorption peaks at 1464 cm^{-1} , 1435 cm^{-1} , and 1407 cm^{-1} belong to -CH- bending vibrations in the carbon chain. Among them, 1464 cm^{-1} is the in-plane bending vibration peak (NCH) of -CH at CH₃-CH₂- in the carbon chain (Xiao et al., 2020b). These absorption bands are common in hydrocarbons. Both the wide absorption band at 1333 cm^{-1} and the absorption peak at 1549

cm^{-1} belong to the stretching vibration of $\text{C}=\text{O}$ ($\nu_{\text{C}=\text{O}}$) in the carboxylate group $-\text{COO}-$, which is also proof of the intercalation of BS-12 to montmorillonite of NB (Lapo et al., 2020).

Comparing the FT-IR spectra of the four samples, the vibration of $\text{Al}-\text{O}(\text{OH})-\text{Al}$ and $\text{Si}-\text{Mg}$ of the clay octahedral in the low-frequency lattice bending vibration band did not change significantly, indicating that, for the composition of silicate in the interlayer domain, changes have taken place, but the basic silicate skeleton vibration has not changed and maintains the original structural state.

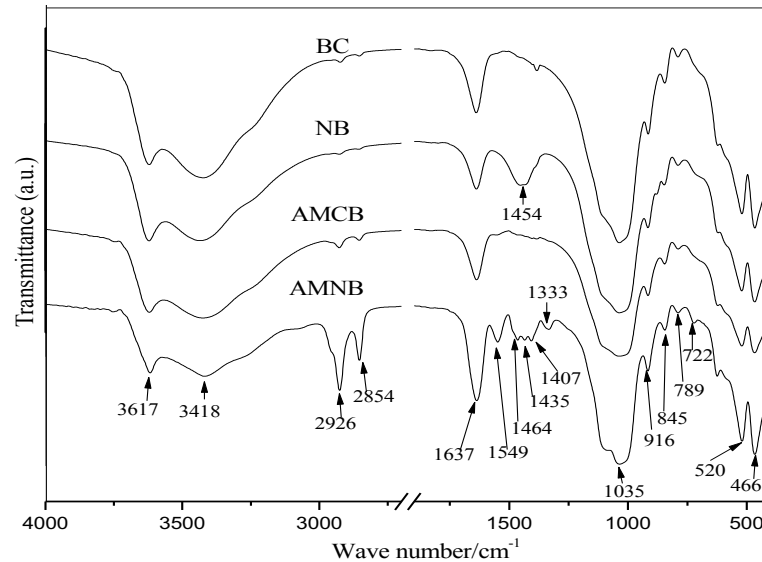


Fig. 9. FT-IR spectra of the four samples

According to the adsorption results and the test results of Fig. 7–9, the sodium modification improved the CEC of NB compared with that of BC, resulting in a stronger negative charge on the NB surface than that of BC. Strong surface electronegativity increases the repulsion between montmorillonite particles, enhances dispersion, and increases the swelling capacity. The replacement of interlayer hydrated calcium ions by sodium ions is the root cause of this series of changes. However, it should be noted that, since the adsorption of NB on AY11 is not an ion exchange adsorption caused by the increase in CEC, the change in the type of interlayer hydrated cations is not the cause of the change in the adsorption performance of bentonite to AY11. The surface of montmorillonite is very hydrophilic. When the two particles are close to each other, a strong hydration repulsion force is generated, which hinders the aggregation of the particles (Yang et al., 2017). The hydration energy of calcium ions between layers of natural calcium bentonite is less than that of sodium ions, so when it is dispersed in water, the hydration repulsion force on the particle surface is lower than that of natural sodium bentonite and sodium-modified bentonite, which is reflected in its lower swelling capacity and poor water absorption (Barast et al., 2017). Under the dual effects of poor dispersibility and negative surface charge, it is extremely difficult for AY11, an organic compound with an anionic group, to come into contact with the surface of the montmorillonite particles, so BC showed extremely poor adsorption to AY11. As shown in Fig. 10, after sodium modification, Na^+ , which has a large hydration energy between the crystalline layers, escapes from the interlayer space when it comes into contact with water, weakening the bonding force between crystal layers, which enables the H_2O molecule to be inserted into the layers and increases the layer spacing sharply, making the mineral particles swell rapidly. On the other hand, each unit cell of montmorillonite contains 0.25–0.60 structural negative charges, so a large number of cations are adsorbed on the surface of montmorillonite. These cations diffuse into the solution in the aqueous solution, forming an electric double layer on the particle surface. The surfaces of adjacent particles are negatively charged and repel each other, which increases the spacing between the particles and causes the volume of the clay particles to expand. The increase in CEC and the increase in the surface negative electricity signify that the number of cations attached to the montmorillonite surface has increased during the sodium modification process, which makes the electric double layer on the surface of the NB particles more repulsive and further improves the swelling performance of

bentonite. Sodium modification increased the swelling capacity of the bentonite several times, released the large internal surface area of the montmorillonite particles and greatly increased the probability of AY11 contacting montmorillonite particles and adsorbing to the montmorillonite surface under the action of van der Waals force (Yang, 2018). Therefore, compared with BC, NB shows a better adsorption capacity for AY11.

According to FT-IR spectroscopy, it was found that the inter-layer organic content of AMCB is limited, while the inter-layer organic content of AMNB is much higher. There are two reasons for this phenomenon. On the one hand, the poor hydration properties of calcium-based bentonite make the interlayer space limited, which is not conducive to the exchange and replacement of calcium ions by BS-12 entering the interlayer. However, the bentonite interlayer domain after sodium modification is fully expanded and the internal surface area is increased, which increases the chance of BS-12 entering the interlaminar region and exchanging with cations. On the other hand, the larger hydration of sodium ions makes it easier for sodium ions to overflow from the interlayer space of Na-modified bentonite than for calcium ions to overflow from the interlayer space of calcium-based bentonite, which increases the probability of being replaced by BS-12. The amphoteric surface modifier BS-12 has a hydrophobic carbon chain and two hydrophilic groups with positive and negative charges, respectively. After modification by BS-12, the hydrophilic group of BS-12 is combined with the surface of bentonite, and its long hydrocarbon chain hydrophobic group extends outward, forming an organic phase on the surface of the bentonite, which makes the surface of the bentonite have a certain degree of hydrophobicity. AY11 molecules are easily adsorbed on the surface of modified bentonite, so the adsorption capacity of the modified bentonite to AY11 is greatly increased compared with unmodified bentonite (Meng et al., 2008).

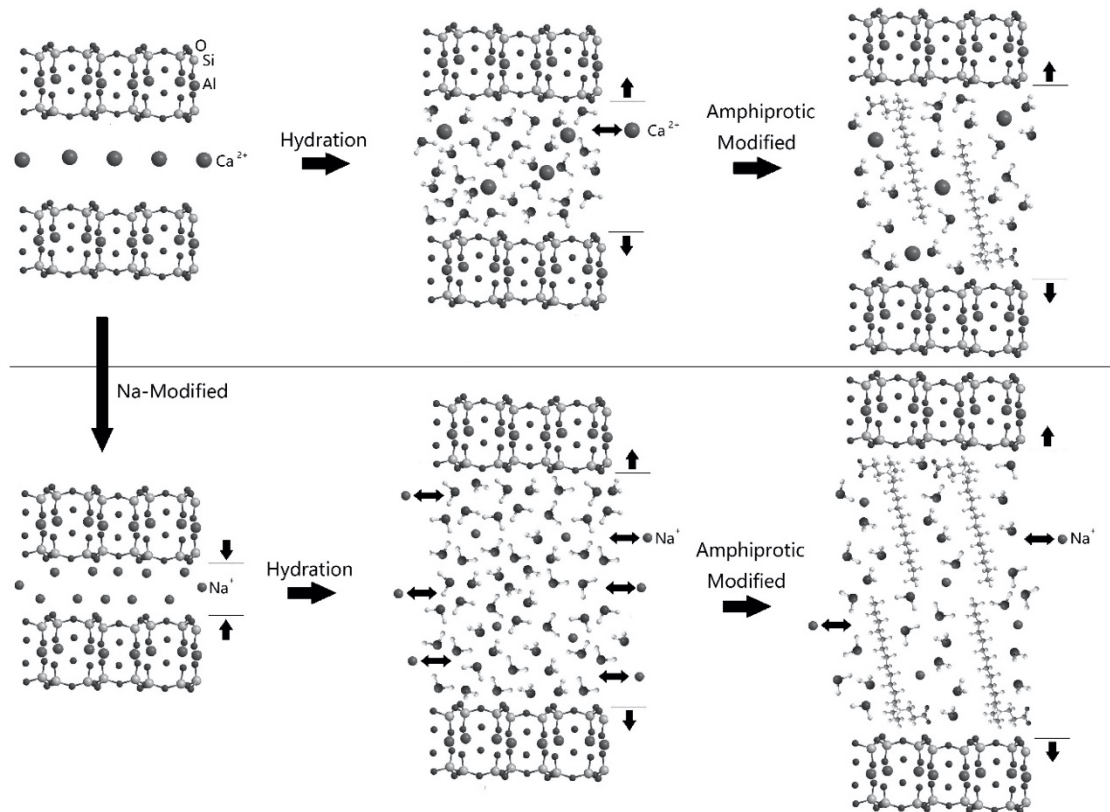


Fig. 10. Schematic of modification mechanism

4. Conclusions

The effects of sodium modification pretreatment on the amphoteric modification of calcium bentonite was studied by the evaluation standard of the adsorbability of anionic dye AY11. Natural calcium bentonite does not absorb anionic dyes easily, but amphoteric modification can improve the adsorption

capacity of anionic dyes, and sodium modification also has the same effect. The adsorption capacity of calcium bentonite can be improved by sodium–amphoteric modification (AMNB), which is evidently better than that of amphoteric organic modified calcium bentonite (AMCB) and sodium modification bentonite (NB). The natural calcium-based bentonite has poor dispersibility and hydration performance, and a large amount of negative charges are accumulated on the particle surface, making it difficult for AY11 to adsorb on the particle surface; therefore it demonstrated poor adsorption performance. The sodium modification expanded the interlayer space and released the internal surface area of the particles, which greatly increased the probability of AY11 contacting with montmorillonite particles and adsorption with montmorillonite under the action of van der Waals force. The adsorption mechanism research shows that the adsorption mechanism of AMNB and AMCN for AY11 is different from that of NB. The adsorption of AY11 by NB takes place on the exterior surface of the adsorbent and proceeds rapidly. BS-12 adsorbs on the bentonite surface through the combination of a hydrophilic group and permanent negative charge on the bentonite surface and replaces a part of the interlayer hydrated cation. Its outwardly extending hydrophobic carbon chain forms an organic phase on the surface of bentonite, with the result that AY11 is adsorbed by the amphoteric bentonite. In the process of amphoteric modification, the pretreatment of sodium modification also played a similarly positive role in the release of interlayer space; however, since the hydration energy of Na^+ is greater than that of Ca^{2+} , when Ca^{2+} is replaced by Na^+ , Na^+ is more likely to escape from the interlayer space and exchange with the modifier. Therefore, the amphoteric bentonite pretreated by sodium modification has a higher organic content in the interlayer than that of amphoteric bentonite without pretreatment, and the hydration performance, dispersion performance, and adsorption performance are significantly improved.

The findings of this investigation suggest that the pretreatment of sodium modification is positive and necessary for sodium–amphoteric modification.

References

- ACEMIOĞLU, B., 2004. *Adsorption of congo red from aqueous solution onto calcium-rich fly ash*. Journal of Colloid and Interface Science. 274(2), 371-379.
- AFOLABI, R.O., ORODU, O.D., EFEVOBOKHAN, V.E., 2017. *Properties and application of nigerian bentonite clay deposits for drilling mud formulation: recent advances and future prospects*. Applied Clay Science. 143, 39-49.
- AMIN, N.K., 2009. *Removal of direct blue-106 dye from aqueous solution using new activated carbons developed from pomegranate peel: adsorption equilibrium and kinetics*. Journal of Hazardous Materials. 165(1-3), 52-62.
- ARELLANO-CÁRDENAS, S., LÓPEZ-CORTEZ, S., CORNEJO-MAZÓN, M., MARES-GUTIÉRREZ, J.C., 2013. *Study of malachite green adsorption by organically modified clay using a batch method*. Applied Surface Science. 280, 74-78.
- ARONSON, J.L., LEE, M., 1986. *K/ar systematics of bentonite and shale in a contact metamorphic zone, cerrillos, new mexico*. Clays and Clay Minerals. 34(4), 483-487.
- BARAST, G., RAZAKAMANANTSOA, A., DJERAN-MAIGRE, I., NICHOLSON, T., WILLIAMS, D., 2017. *Swelling properties of natural and modified bentonites by rheological description*. Applied Clay Science. 142, 60-68.
- BELOUSOV, P.E., KRUPSKAYA, V.V., 2019. *Bentonite clays of russia and neighboring countries*. Georesursy. 21(3), 79-90.
- BENITO, R., GARCIA-GUINEA, J., VALLE-FUENTES, F.J., RECIO, P., 1998. *Mineralogy, geochemistry and uses of the mordenite-bentonite ash-tuff beds of los escullos, almería, spain*. Journal of Geochemical Exploration. 62(1-3), 229-240.
- BIANCHI, A.E., FERNÁNDEZ, M., PANTANETTI, M., VIÑA, R., TORRIANI, I., SÁNCHEZ, R.M.T., PUNTE, G., 2013. *Odtma+ and hdtma+ organo-montmorillonites characterization: new insight by waxes, saxs and surface charge*. Applied Clay Science. 83-84, 280-285.
- DAWODU, F.A., AKPOMIE, K.G., 2014. *Simultaneous adsorption of ni(ii) and mn(ii) ions from aqueous solution unto a nigerian kaolinite clay*. Journal of Materials Research and Technology. 3(2), 129-141.
- EBRAHIMI, A., ARAMI, M., BAHRAMI, H., PAJOOTAN, E., 2013. *Fish bone as a low-cost adsorbent for dye removal from wastewater: response surface methodology and classical method*. Environmental Modeling & Assessment. 18(6), 661-670.
- GEORGIN, J., DOTTO, G.L., MAZUTTI, M.A., FOLETTO, E.L., 2016. *Preparation of activated carbon from peanut shell*

- by conventional pyrolysis and microwave irradiation-pyrolysis to remove organic dyes from aqueous solutions.* Journal of Environmental Chemical Engineering, 4(1), 266-275.
- General administration of quality supervision, inspection and quarantine of the People's Republic of China and Standardization administration of the People's Republic of China, *Method for the determination of whiteness, acidity and swelling capacity of granular bentonite for export*, SNT 0990-2001
- General administration of quality supervision, inspection and quarantine of the People's Republic of China and Standardization administration of the People's Republic of China, *Bentonite*, GB/T 20973-2007
- HAGHSERESHT, F., WANG, S., DO, D.D., 2009. *A novel lanthanum-modified bentonite, phoslock, for phosphate removal from wastewaters.* Applied Clay Science. 46(4), 369-375.
- HAMEED, B.B., ISMAIL, Z.Z., 2020. *Biodegradation of reactive yellow dye using mixed cells immobilized in different biocarriers by sequential anaerobic/aerobic biotreatment: experimental and modelling study.* Environmental Technology., 1-20.
- HO, Y.S., MCKAY, G., 1999. *Pseudo-second order model for sorption processes.* Process Biochemistry. 34(5), 451-465.
- HOU, M., MA, C., ZHANG, W., TANG, X., FAN, Y., WAN, H., 2011. *Removal of rhodamine b using iron-pillared bentonite.* Journal of Hazardous Materials. 186(2-3), 1118-1123.
- KIRALI, E.G., LAÇIN, O., 2006. *Statistical modelling of acid activation on cotton oil bleaching by turkish bentonite.* Journal of Food Engineering. 75(1), 137-141.
- LAPO, B., BOU, J.J., HOYO, J., CARRILLO, M., PEÑA, K., TZANOV, T., SASTRE, A.M., 2020. *A potential lignocellulosic biomass based on banana waste for critical rare earths recovery from aqueous solutions.* Environmental Pollution. 264, 114409.
- LEODOPOULOS, C., DOULIA, D., GIMOHOPOULOS, K., 2015. *Adsorption of cationic dyes onto bentonite.* Separation & Purification Reviews. 44(1), 74-107.
- LI, Y., DU, Q., LIU, T., QI, Y., ZHANG, P., WANG, Z., XIA, Y., 2011. *Preparation of activated carbon from enteromorpha prolifera and its use on cationic red x-grl removal.* Applied Surface Science. 257(24), 10621-10627.
- LUM, P.T., FOO, K.Y., ZAKARIA, N.A., PALANIANDY, P., 2020. *Ash based nanocomposites for photocatalytic degradation of textile dye pollutants: a review.* Materials Chemistry and Physics. 241, 122405.
- MADEJOVÁ, J., 2003. *Ftir techniques in clay mineral studies.* Vibrational Spectroscopy. 31(1), 1-10.
- MALIK, P.K., 2004. *Dye removal from wastewater using activated carbon developed from sawdust: adsorption equilibrium and kinetics.* Journal of Hazardous Materials. 113(1-3), 81-88.
- MENG, Z., ZHANG, Y., ZHANG, Z., 2008. *Simultaneous adsorption of phenol and cadmium on amphoteric modified soil.* Journal of Hazardous Materials. 159(2-3), 492-498.
- MENG, Z., ZHANG, Y., WANG, G., 2007. *Sorption of heavy metal and organic pollutants on modified soils.* Pedosphere. 17(2), 235-245.
- MITCHELL, C.E., ADHYA, S., BERGSTRÖM, S.M., JOY, M.P., DELANO, J.W., 2004. *Discovery of the ordovician millbrig k-bentonite bed in the trenton group of new york state: implications for regional correlation and sequence stratigraphy in eastern north america.* Palaeogeography, Palaeoclimatology, Palaeoecology. 210(2-4), 331-346.
- Ministry of Ecology and Environment of the People's Republic of China, *Discharge standards of water pollutants for dyeing and finishing textile industries*, GB 4287-2012
- Ministry of Ecology and Environment of the People's Republic of China, *Self-monitoring technology guidelines for pollution sources - Textile and dyeing industry*, HJ 879-2017
- Ministry of Ecology and Environment of People's Republic of China, *Technical guidelines of accounting method for pollution source intensity textile and dyeing industry*, HJ 990-2018
- Ministry of Industry and Information Technology of the People's Republic of China, 2019. *List of enterprises in accordance with the standards of dyeing industry (2017 edition).*
- National Bureau of Statistics of People's Republic of China, 2019. *China statistical yearbook-2019.* China statistics press.
- National Bureau of Statistics of the People's Republic of China, 2020. *Statistical communiqué of the people's republic of china on national economic and social development 2019.*
- OLIVEIRA, J.M.S., de LIMA E SILVA, M.R., ISSA, C.G., CORBI, J.J., DAMIANOVIC, M.H.R.Z., FORESTI, E., 2020. *Intermittent aeration strategy for azo dye biodegradation: a suitable alternative to conventional biological treatments?* Journal of Hazardous Materials. 385, 121558.
- ÖTKER, H.M., AKMEHMET-BALCIOĞLU, I., 2005. *Adsorption and degradation of enrofloxacin, a veterinary antibiotic on natural zeolite.* Journal of Hazardous Materials. 122(3), 251-258.

- PERIASAMY, K., NAMASIVAYAM, C., 1995. *Removal of nickel(ii) from aqueous solution and nickel plating industry wastewater using an agricultural waste: peanut hulls*. Waste Management. 15(1), 63-68.
- PURKAIT, M., DASGUPTA, S., DE, S., 2006. *Micellar enhanced ultrafiltration of eosin dye using hexadecyl pyridinium chloride*. Journal of Hazardous Materials. 136(3), 972-977.
- RAWAJFIH, Z., NSOUR, N., 2006. *Characteristics of phenol and chlorinated phenols sorption onto surfactant-modified bentonite*. Journal of Colloid and Interface Science. 298(1), 39-49.
- SAIDI, R., TLILI, A., FOURATI, A., AMMAR, N., OUNIS, A., JAMOUCSI, F., 2012. *Granulometric distribution of natural and flux calcined chert from ypresian phosphatic series of gafsa-metlaoui basin compared to diatomite filter aid*. Iop Conference Series: Materials Science and Engineering. 28, 12027.
- SANTOS, S.S.G., FRANÇA, D.B., CASTELLANO, L.R.C., TRIGUEIRO, P., SILVA FILHO, E.C., SANTOS, I.M.G., FONSECA, M.G., 2020a. *Novel modified bentonites applied to the removal of an anionic azo-dye from aqueous solution*. Colloids and Surfaces A: Physicochemical and Engineering Aspects. 585, 124152.
- SANTOS, S.S.G., FRANÇA, D.B., CASTELLANO, L.R.C., TRIGUEIRO, P., SILVA FILHO, E.C., SANTOS, I.M.G., FONSECA, M.G., 2020b. *Novel modified bentonites applied to the removal of an anionic azo-dye from aqueous solution*. Colloids and Surfaces A: Physicochemical and Engineering Aspects. 585, 124152.
- SLANÝ, M., JANKOVIČ, =., MADEJOVÁ, J., 2019. *Structural characterization of organo-montmorillonites prepared from a series of primary alkylamines salts: mid-ir and near-ir study*. Applied Clay Science. 176, 11-20.
- VANHULLE, S., TROVASLET, M., ENAUD, E., LUCAS, M., TAGHAVI, S., van der LELIE, D., van AKEN, B., FORET, M., ONDERWATER, R.C.A., WESENBERG, D., AGATHOS, S.N., SCHNEIDER, Y., CORBISIER, A., 2008. *Decolorization, cytotoxicity, and genotoxicity reduction during a combined ozonation/fungal treatment of dye-contaminated wastewater*. Environmental Science & Technology. 42(2), 584-589.
- VIVES, M.T., BALAGUER, M.D., GARCÍA, S., GARCÍA, R., COLPRIM, J., 2003. *Textile dyeing wastewater treatment in a sequencing batch reactor system*. Journal of Environmental Science and Health, Part A. 38(10), 2089-2099.
- WANG, T., TANG, X., ZHANG, S., ZHENG, J., ZHENG, H., FANG, L., 2020. *Roles of functional microbial flocculant in dyeing wastewater treatment: bridging and adsorption*. Journal of Hazardous Materials. 384, 121506.
- WANG, Z., XUE, M., HUANG, K., LIU, Z., 2011. *Textile dyeing wastewater treatment*. InTech, Rijeka, Croatia.
- XIAO, F., YAN, B., ZOU, X., CAO, X., DONG, L., LYU, X., LI, L., QIU, J., CHEN, P., HU, S., ZHANG, Q., 2020a. *Study on ionic liquid modified montmorillonite and molecular dynamics simulation*. Colloids and Surfaces A: Physicochemical and Engineering Aspects. 587, 124311.
- XIAO, F., YAN, B., ZOU, X., CAO, X., DONG, L., LYU, X., LI, L., QIU, J., CHEN, P., HU, S., ZHANG, Q., 2020b. *Study on ionic liquid modified montmorillonite and molecular dynamics simulation*. Colloids and Surfaces A: Physicochemical and Engineering Aspects. 587, 124311.
- YANG, Y., SUN, C., LIN, B., HUANG, Q., 2020. *Surface modified and activated waste bone char for rapid and efficient vocs adsorption*. Chemosphere. 256, 127054.
- YUAN, Y., NING, X., ZHANG, Y., LAI, X., LI, D., HE, Z., CHEN, X., 2020. *Chlorobenzene levels, component distribution, and ambient severity in wastewater from five textile dyeing wastewater treatment plants*. Ecotoxicology and Environmental Safety. 193, 110257.
- ZHENG, R., GAO, H., REN, Z., CEN, D., CHEN, Z., 2017. *Preparation of activated bentonite and its adsorption behavior on oil-soluble green pigment*. Physicochemical Problems of Mineral Processing. 53(2), 829-845.
- ZHU, K., JIA, H., WANG, F., ZHU, Y., WANG, C., MA, C., 2016. *Efficient removal of pb(ii) from aqueous solution by modified montmorillonite/carbon composite: equilibrium, kinetics, and thermodynamics*. Journal of Chemical and Engineering Data. 62(1), 333-340.
- ZHUANG, X., WAN, Y., FENG, C., SHEN, Y., ZHAO, D., 2009. *Highly efficient adsorption of bulky dye molecules in wastewater on ordered mesoporous carbons*. Chemistry of Materials. 21(4), 706-716.
- LI, T., 2012. *Equilibrium adsorption characteristics of amphoteric modified bentonites to cd (ii) and phenol*. Northwest A&F University, p. 69.
- LIANG, L., 2020. *Dyeing of annual inventory: green development into industry consensus*. China Textile. (01), 28.
- PANG, Y., DING, Y., SUN, B., LV, X., 2008. *Preparation and physicochemical properties of bentonite modified by cetyl trimethyl ammonium*. Journal of Liaoning Normal University (Natural Science Edition). (03), 322-325.
- REN, S., MENG, Z., WANG, T., ZHANG, Y., TIAN, K., 2018. *Comparison of amphoteric-cationic and amphoteric-anionic modified magnetic bentonites: characterization and sorption capacity oh phenol*. Environmental science. Environmental Science. 39(01), 187-194.
- SUN, H., ZHU, L., 2010. *The performance of the hdtma-aet modified bentonite as a sorbent for cd and p-nitrophenol*. Acta

- Scientiae Circumstantia. 30(05), 1037-1042.
- WU, X., YUAN, P., PENG, C., 2016. *The development status, main problems and suggestions of bentonite industry in china.* The World of Building Materials. 03(37), 27-30.
- YAN, P., HAO, W., GAO, T., 2004. *Chemistry of fine chemicals.* Chemical Industry Press, Beijing.
- YANG, Z., 2018. *Quantum chemical study on inhibiting the expansion and dissolution of montmorillonite in slime water system.* China University of Mining & Technology, p. 146.
- YANG, Z., LIU, W., JIAO, X., REN, Z., 2017. *Calculation of electrostatic interaction energy by using zeta potential in montmorillonite dispersion system.* Journal of china coal society. 42(06), 1572-1578.